Optics & Laser Technology 180 (2025) 111479

Contents lists available at ScienceDirect

Optics and Laser Technology

journal homepage: www.elsevier.com/locate/optlastec

Full length article

Femtosecond laser removal of antifouling paints on glass fibre reinforced plastic used in maritime industry

Alicia Moreno-Madariaga [a,*], Aurora Lasagabáster-Latorre [b], María L. Sánchez Simón [c], Javier Lamas [a], Alberto Ramil [a], Ana J. López [a]

[a] Campus Industrial de Ferrol, Laboratorio de Aplicaciones Industriales del Láser, CITENI, Universidade de Coruña, Spain
[b] Dpto Química Orgánica I, Facultad de Óptica y Optometría, Universidad Complutense de Madrid, Spain
[c] Campus Industrial de Ferrol, Escuela Politécnica de Ingeniería de Ferrol, Universidade da Coruña, Spain

ARTICLE INFO

Keywords:
Femtosecond laser
Laser cleaning
Antifouling paint
GFRP
Maritime environment

ABSTRACT

In this work we investigated the use of ultrashort laser pulses to clean antifouling paint from samples of glass fibre reinforced polymer (GFRP), a composite material widely used in shipbuilding. Samples were prepared with two types of paint, self-polishing and hard matrix, according to the scheme used in the shipyard. The paints and the GFRP substrate were characterised by Fourier transform infrared (FTIR) spectroscopy and scanning electron microscopy (SEM) with energy dispersive X-ray spectrometry (EDS). The effectiveness of the cleaning treatment and the effects on the substrate were evaluated by optical microscopy, interferometric microscopy, SEM-EDS and FTIR spectroscopy. The results indicate that satisfactory cleaning was achieved with controlled removal of unwanted layers without damaging or chemically altering the polymer bulk. The surfaces were also evaluated by SEM and interferometric microscopy to characterise morphological changes, and their wettability was characterised by contact angle measurements. In addition, the results were compared with those obtained by the conventional mechanical method (paint scraping and sanding). A roughening of the laser cleaned surfaces was observed compared to untreated surfaces as well as compared to mechanically cleaned surfaces. Laser treatment caused a decrease in wettability; sanded surfaces showed comparable behaviour. This study demonstrates the potential of femtosecond lasers for safe and effective cleaning of GFRP substrates in a more environmentally friendly manner.

1. Introduction

Composite materials are extensively used in maritime applications due to their corrosion resistance, lightweight, and ability to manufacture complex shapes without expensive tooling, making them advantageous. Glass fibre reinforced plastics (GFRP) are widely used for the hulls of pleasure boats, military crafts, fishing boats, and catamarans. They are also used in Marine Renewable Energy Production for elements such as turbine blades and propellers [1].

Biofouling is a significant issue for the maritime industry, involving the attachment of marine flora and fauna to submerged structures [2]. When marine organisms attach to the hull of ships or naval vessels, they can increase frictional resistance, reducing speed and manoeuvrability, increasing fuel consumption and corrosion damage, and posing a biosecurity risk. In addition, hull fouling can increase the frequency of drydocking, resulting in significant economic losses [3,4]. Therefore, it is important to prevent such attachments [5,6].

One of the most commonly used preventive methods nowadays is the application of antifouling paints that contain biocides. These biocides act as repellents or poisons for potential settling organisms. In the EU, antifouling products are regulated under the Biocidal Products Regulation (BPR), which stipulates that the recommended dose should be the minimum necessary to achieve the desired effect. Therefore, periodic cleaning and repainting of the surface are necessary to maintain antifouling performance. Currently, antifouling paints are typically removed using mechanical methods such as hydroblasting, sandblasting, scraping, or sandpapering. However, these methods generate paint waste and/or wastewater that is highly contaminated with metals and other biocides; and even biological risks when in-water cleaning systems remove hull fouling [7–10]. So that, it is important to find alternative methods that are more environmentally friendly [11–14].

In this context, the laser cleaning technique is presented as a highly

* Corresponding author.
E-mail address: alicia.moreno@udc.es (A. Moreno-Madariaga).

https://doi.org/10.1016/j.optlastec.2024.111479
Received 10 April 2024; Received in revised form 18 June 2024; Accepted 13 July 2024
Available online 18 July 2024

effective alternative for removing various types of paints and coatings. Laser cleaning has been applied in various industrial fields, including aerospace and automotive [15–19], and even for the removal of radioactive contaminants [20]. It has also been used in fields such as dentistry [21] and heritage conservation [22–25]. Compared to conventional cleaning methods, laser cleaning offers several advantages. It is a selective, non-contact, and environmentally friendly technique [26]. When combined with industrial robots, laser technology can accurately clean contaminants in large and complex structures, which greatly improves quality and efficiency [27–32].

Short pulse lasers with pulse durations in the nanosecond or microsecond range are commonly used for cleaning, and research on paint removal has mainly focused on metal matrices [33–38], with relatively little research reported on fiber reinforced composites [39–41]. The main challenge in laser processing of composites is the suppression of thermal damage to the bulk resin or load-bearing fibres [42], because of the the difference in thermophysical properties of fibres and matrices [43]. In this sense, studies on the effects of nanosecond lasers with wavelengh in the IR and UV rarge on fibre reinforced plastics showed that in both regimes the thermal effect of the laser is the dominant cleaning mechanism in paint stripping; even in the UV range where photochemical mechanisms are involved in addition with thermal stress [44–46]. On the other hand, with ultra-short pulsed lasers (picosecond or femtosecond range), the interaction between the laser and the material is based on electrostatic processes and the pulse duration is shorter than the time required for heat to diffuse through the material [47]. As a result, there is minimal heat transfer into the bulk of the material and they are therefore increasingly used, particularly for processing heat-sensitive materials such as cultural heritage objects [48–52] or composites [53–56]. Focusing on laser processing of GFRP composites, many scholars have studied GFRP laser cutting and drilling and found that thermal damage is reduced by minimisation of irradiation time, furthermore using ultrashort pulses, the pulse duration and wavelength had a great impact on the heat-affected zone (see Bhaskar et al. [57] and references therein); however, to the best of our knowledge, few literatures have reported paint removal on GFRP, and in such cases IR lasers have been used. [58].

So that, although studies on UV laser surface treatment of composites have shown promising results [59,60], their use in automation processes or integration with robots is limited because UV lasers cannot be guided by conventional silica based optical fibre [61]. Infrared lasers, on the other hand, can be guided through an optical fibre and are therefore very suitable for automation [35,62,63]. This aspect is of great importance when considering the applicability of this study in industrial fields, given the size and shape of the surfaces to be cleaned, ship hulls and other elements with very different sizes and shapes, which can, however, be tackled thanks to the technological advances in high power ultrafast fiber laser systems [41,64,65].

In the context of maritime applications, there is limited literature on laser cleaning of paints or coatings, and where such references exist, they typically involve the use of nanosecond lasers [66–72]. Furthermore, due to the fact that functional paints or coatings are made up of a combination of different pigments, resins and other additives designed to improve specific properties, the response of different types of paint to laser irradiation can be a challenge [24,48,73,74].

This work investigates the use of ultrashort pulse laser cleaning technology for removing antifouling paints from GFRP surfaces used in shipbuilding. The study focuses on two commonly used antifouling coatings: self-polishing and hard matrix. Prior to laser cleaning, the paints and GFRP surface were characterized, and the efficiency of the laser ablation process was evaluated. The paint removal efficiency and effects on the substrate, including its chemical composition, surface roughness, and wettability, were used to characterize the results. These factors could potentially impact the repainting procedure. Additionally, the study compared the results of decoating laser with those of the conventional mechanical method.

2. Materials and methods

2.1. Samples preparation

The composite samples utilised in this study were prepared in the shipyard using the manual laminating method, which consists of adding successive layers of resin and fibre in a mould. The process of constructing a hull laminate begins with a mould that has been impregnated with release agents (wax). Fibreglass mats, which have been impregnated with polyester resin, are then applied layer by layer and welded together once the resin has cured. To create the external surface of the hull, a layer of gel-coat was applied before layering the part [75,76]. The resin used, identified as POLYCOR ISO NPG PA and manufactured by Polynt Composites, is a white isophthalic neopentylglycol chosen for its high resistance to water and blistering. After demoulding, the gel-coat surface was sanded to remove all traces of release agent and achieve good mechanical anchorage for the painting scheme. A white primer coat was applied to improve mechanical adhesion for the antifouling paint application. Additionally, the primer provides protection, especially for boats laminated with polyester. Finally, two coats of antifouling paint were applied. All coats were applied using a roller.

Two types of Hempel antifouling coatings were used in this study: a red self-polishing coating, referred to as 'red-SP', and a hard or insoluble matrix antifouling white paint, identified as 'white-HM'. After the painting process was completed, the glass fibre reinforced plastic (GFRP) laminate, which was approximately 8 mm thick, was cut into flat sheets measuring (100 × 100) mm^2.

To be used as a reference, unpainted gel-coat samples were also available. Prior to applying analytical techniques, the gel-coat surfaces were cleaned with detergent-based cleaners and a special solvent to remove all traces of the release agent.

To compare the effects of laser treatments with those of the conventional mechanical method, we reproduced the manual process in the laboratory. We used a paint scraper to clean the gel-coat surfaces and then abraded them with 120 grit sandpaper using an orbital sander to obtain a good mechanical grip for the application of the new paint. Finally, we rinsed the prepared surfaces with fresh water to remove dust and sandpaper residue.

2.2. Femtosecond laser system

The samples were subjected to laser irradiation to completely remove the antifouling paint while minimizing damage to the gel-coat surface. The laser used was the Spirit system from Spectra Physics, emitting at a wavelength of 1040 nm and with a pulse width of less than 400 fs. The laser output had a near-Gaussian intensity profile ($M^2 < 1.2$) and a beam diameter of 1.5 mm at the laser head exit. The laser beam has a horizontal polarisation (>100:1). The pulse rate can be adjusted from a single shot up to 1 MHz, with a maximum pulse energy of 40 μJ at 100 kHz. The maximum average output power exceeds 4 W. To scan the laser beam in the X-Y direction, a two-mirror galvanometric scanner (Raylase SuperscanIII-15) was utilised. The beam was focused to a diameter of 30 μm using an F-theta objective lens with a focal length of 160 mm. At the working plane, the beam polarisation is parallel to the Y direction.

The samples undergo processing in ambient air, and the laboratory's extraction system is utilized to eliminate gases and particles produced during ablation. A scheme of the experimental setup used is shown in Fig. 1.

2.3. Analytical techniques

The surfaces were characterized before and after laser processing using various techniques:

2.3.1. Optical microscopy

To assess the continuity of the coating layers and measure their

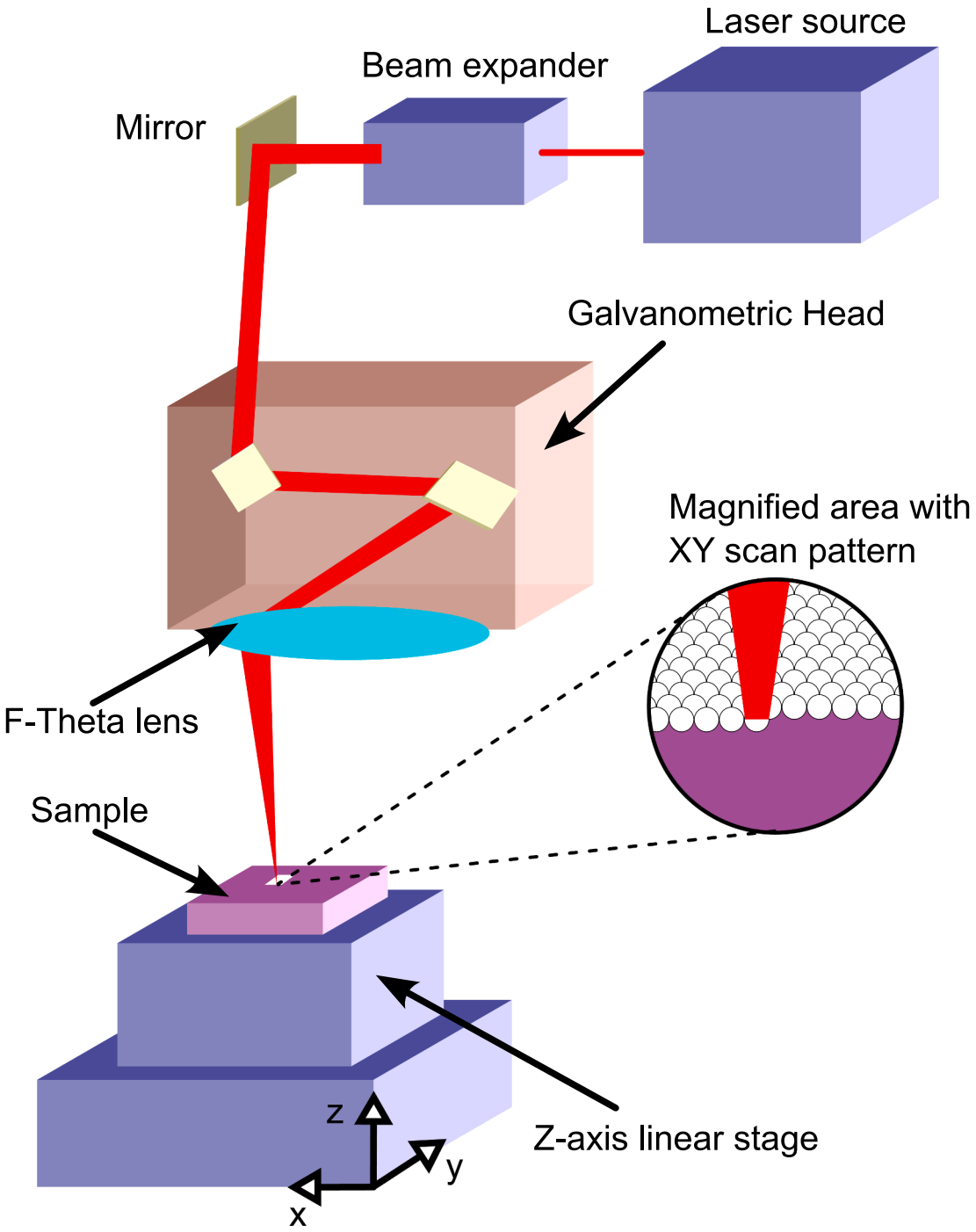

Fig. 1. Scheme of the experimental setup.

thickness, as well as to obtain a first qualitative assessment of the laser's effectiveness in removing paint, we used a Nikon Eclipse L150 on polished cross-sections of fresh samples.

2.3.2. Scanning electron microscopy (SEM)

The study employed a JEOL JSM-7200F scanning electron microscope (SEM) with energy dispersive X-ray spectrometry (EDS) capabilities in both secondary electrons (SE) and back-scattered electrons (BSE) modes. The samples were carbon-coated using a Cressintong 208HR turbo molecular pump. Optimal observation conditions were achieved with an accelerating voltage of 15 kV and a working distance of 9–10 mm. Analyses were conducted on both the surface and cross-section of the samples.

2.3.3. Fourier transform infrared spectroscopy FTIR

The Fourier Transformed Infrared (FTIR) data were performed on a Jasco 4700 spectrometer coupled with an IRT-7100 Microscope equipped with an MCT detector. The spectra were conducted in the Attenuated Reflectance Mode (ATR) by using the ATR-5000-SS Clear-View ATR objective with a ZnS prism. At least three individual spectra were collected for each sample area between 3600 and 650 cm^{-1}. Each spectrum was compiled from 64 scans with a resolution of 4.0 cm^{-1}. The original paints, the gel-coat and a completely cleaned area were also examined in the conventional ATR spectrometer between 3800 and 550 cm^{-1}. All the spectra were analysed using the Bruker OPUS® software version 5.5. They were subjected to baseline, ATR correction and normalised with respect to the C–H stretching bands (3000–2710 cm^{-1}).

This group of bands has been selected owing to the fact that they are the least affected by the laser cleaning treatment.

2.3.4. Interferometric microscopy

The surface texture was characterized using a Zygo NewView 600 profilometer with a 20x objective (field of view 349 μm × 262 μm, resolution 640 × 480 pixels, Z-scan resolution 0.1 nm). Scientific Python was used for data processing, analysis, and visualization. Areal roughness parameters were used to characterize the surface roughness before and after paint removal, following standard UNE-EN ISO [77].

2.3.5. Contact angle measurement

To assess surface wettability, we measured the static contact angle using a Krüss Drop Shape Analyzer-DSA25 with an automatic dosage system and a Guppy PRO F-032B CCD camera. We followed the sessile drop method outlined in Standard UNE-EN [78] and measured the static contact angles of four 4 μL deionized water droplets.

3. Results and discussion

3.1. Samples characterization

Fig. 2 displays optical microscope images of the cross sections of the samples, revealing the distinct layers of the laminate coating system. The thicker GFRP layer is located at the bottom. It is evident that the paint layer's continuity is comparable in both cases, red-SP and white-HM, but with varying thicknesses. The mean value for the red paint is (78.9 ± 8.7) μm, while for the white paint, it is (100.0 ± 9.0) μm. The thickness of the intermediate primer is (29.6 ± 2.5) μm in both cases. The gel-coat layer has a thickness of (193.7 ± 15.7) μm for the red-SP sample and (128.1 ± 7.5) μm for the white-HM one.

The composition determination of both the gel-coat and the antifouling paint was carried out by ATR-FTIR and SEM-EDS. Fig. 3 shows the normalised ATR-FTIR spectra of the gel-coat and the original red and white paints. The band assignments are described in detail in Table 1. In coherence with the composition of POLYCOR ISO NPG PA, the spectral bands of the gel-coat correspond to an aromatic polyester resin, specifically indicated by the presence of the carbonyl (C=O) and asymmetric C-O-C stretching bands of the ester groups at 1723 and 1230 cm^{-1}, respectively. The presence of the isophthalic moiety is

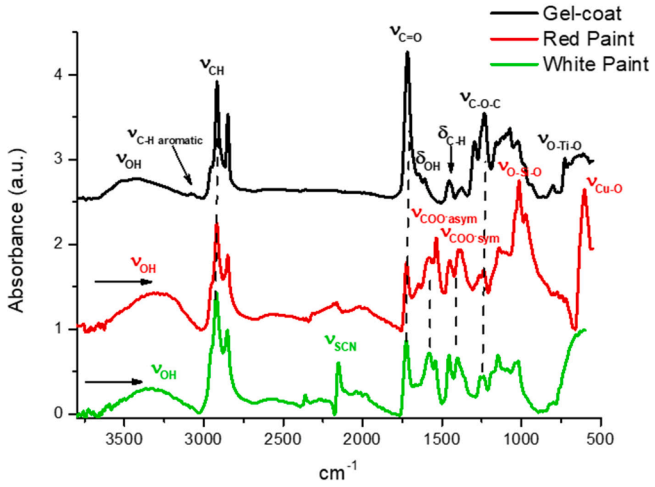

Fig. 3. Normalised ATR-FTIR spectra of the gel-coat and the red and white paints. (For interpretation of the references to color in this figure legend, the reader is referred to the web version of this article.)

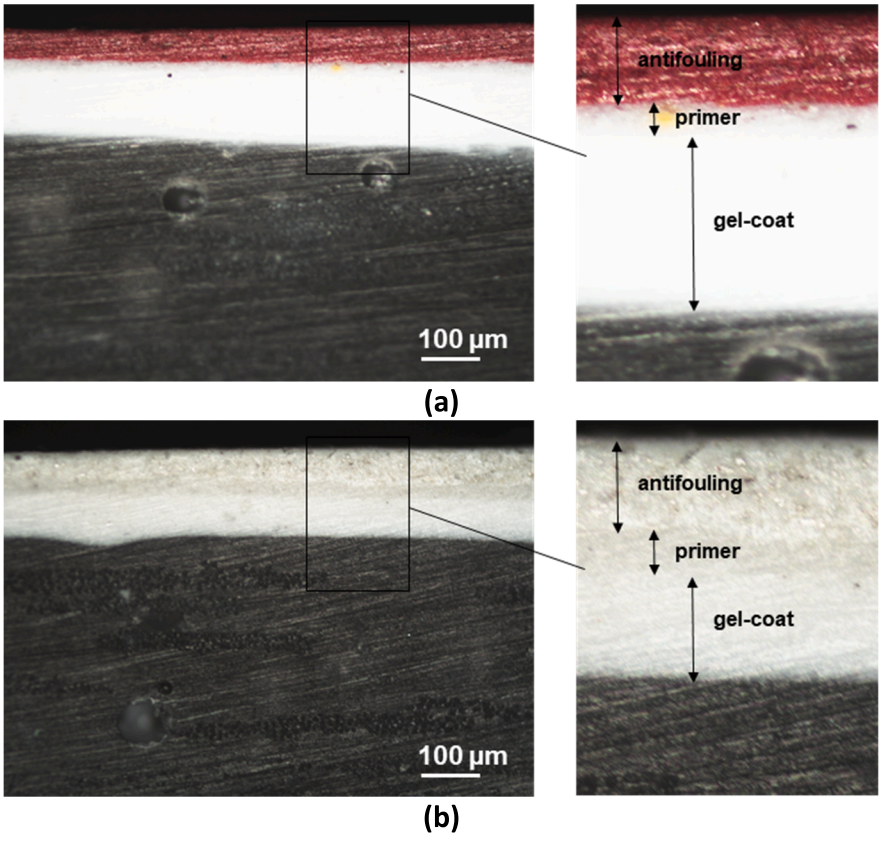

Fig. 2. Optical microscopy images (10x) of cross sections of the red-SP (a) and white-HM (b) samples. (For interpretation of the references to color in this figure legend, the reader is referred to the web version of this article.)

Table 1
Assignment of the infrared absorption bands of the normalised spectra of the original materials.

Wavenumber (cm^{-1})	Group vibration	Origin
3600–3100	OH stretching	Water molecules
3074	aryl CH stretching	Aromatic rings, Gel-coat
2954	CH_3 asym. stretching	Polyester and polyacrylic resin
2926	CH_2 asym. stretching	Polyester and polyacrylic resin
2854	CH_3 CH_2 sym. stretching	Polyester resin, Gel-coat
2155	SCN stretching	Copper(I) thiocyanate biocide
1723	C=O stretching	Polyester and polyacrylic resin
1646	OH bending	Water molecules
1610	C=C aromatic stretching	Aromatic rings, Gel-coat
1583/1542*, 1578/ 1536**	Metal carboxylate COO– asym. stretching	Metal complex, polyacrylic resin
1457	C–H scissoring of CH_2	Polyester and polyacrylic resin
1405*, 1397**	Metal carboxylate COO-sym. stretching	Metal complex, polyacrylic resin
1230	C-O-C asymmetric stretching	Polyester and polyacrylic resin
1230	Si-CH_3 bending	Silanes, imprinting layer
1145	C-O-C symmetric stretching	Polyester and polyacrylic resin
1015	Si-O-Si stretching	SiO_2, silanes
973	Si-O-C, Cu–O	SiO_2, Cu_2O
821	$Si(CH_3)_2$ rocking	Silanes, imprinting layer
804	Skeletal vibrations	Polyester and polyacrylic resin
727	Ti-O stretching	Gel-coat
676		Pigment
604**	Cu–O bond	Cu_2O Biocide pigment
red ** and white* paint		

confirmed by the small bands at 3074 and 1610 cm^{-1} ascribed to C–H and C=C stretching in aromatic rings, respectively [79]. Adsorbed water is revealed by the absorption bands associated with the O–H stretching and bending vibrations at 3600–3000 cm^{-1} and 1646 cm^{-1}, respectively.

An FTIR analysis between 4000 and 600 cm^{-1} does not unambiguously detect most inorganic elements. The presence of Ti (11.8 %), Si (3.5 %), Mg (1.7 %) and Al (0.5 %) is revealed by SEM-EDS elemental analyses. With this fact in mind the medium-intensity band at 727 cm^{-1} may be ascribed to the Ti-O stretching of TiO_2; this oxide is added as a white pigment for providing maximum whiteness and opacity, besides UV protection [80]. Furthermore, although SEM elemental analysis detects Si, the relatively low intensity of the band at 1027 cm^{-1} (normally a very strong band attributed to O-Si-O stretching vibrations) [81], may be due to the limitations of the ATR mode in heterogeneous samples, due to the shallow depth of penetration of the radiation; therefore, the analysis is limited to the upper few microns of the surface. The presence of Si may be due to silicate particles (SiO_2) frequently included to enhance the coating's mechanical properties [81]. At any rate, these instances highlight the restrictions of FTIR and the need to combine several techniques in any investigation of complex mixtures of unknown materials.

Concerning the spectra of the red and white paints compared in Fig. 3, they consist mostly of the binder plus bands assigned to metal complexes, pigments used as biocides and other fillers (Table 1). FTIR spectra reveal that the binders of both paints consist of blends or co-polymers of acrylate esters and acrylic acid. Both paints exhibit strong metal carboxylates bands (CO_2^-) formed by the reaction of the carboxylic acid groups of the binder with the metals present in the aforementioned fillers, often metal oxides such as Cu_2O, red colored biocide probably the main additive in the red paint, and ZnO, frequently synergistically combined with copper compounds [82,83]. Specifically, the strong peaks in the region 1585–1540 cm^{-1} and the bands in the range 1460–1390 cm^{-1} are due to the asymmetric and symmetric stretching vibrations of the aforementioned CO_2^- groups, respectively [81]. These carboxylate bands are more intense in the red paint than in the white paint. Besides, the broad bands between 3600–3100 cm^{-1}, due to the stretching of hydroxyl groups, is shifted to lower wavenumbers in the red-SP compared to the white-HM, indicating stronger hydrogen-bonding.

Further, the red paint spectrum exhibits stronger bands in the range between 1094–1010 and 974 cm^{-1} which can be assigned the stretching of O-Si-O bonds of silicate (SiO_2) [84]. Nevertheless, copper oxide (Cu_2O) also contributes to the 974 cm^{-1} band intensity [85,86]. In addition, the spectrum of the red paint exhibits a strong band centered at 604 cm^{-1}, which may be allotted to the Cu-bond in Cu_2O, although this band is shifted to lower wavenumbers compared to literature [87]. By contrast, the main absorption of ZnO occurs below 600 cm^{-1}, which is out of the detection range of the FTIR spectrometer [88]. Finally, the biocide Copper(I) thiocyanate (CuSCN) is unambiguously identified in spectrum of the white paint due to the band at 2155 cm^{-1}, ascribed to the stretching vibration of the SCN^- group [89]. This band is absent in the red paint.

To complete the identification of the paint compositions, the SEM-EDS elemental analyses of the red paint detected Cu (4.5 %), Zn (3.9 %), Si (0.8 %) and S (0.8 %). These results confirm the synergistic combination of the biocides Cu_2O and ZnO, being S a frequent impurity present in ZnO. In relation with the white paint, the elemental analysis revealed Cu (3.8 %), S (2.2 %), Zn (12.1 %), Ti (9.9 %) and Si (1.1 %). Further, the coincidence of the color mapping distributions of Cu and S elements ratify the presence of Copper(I) thiocyanate as biocide; similar to the red paint, ZnO is combined with a copper compound to synergistically increase antifouling effects and TiO_2 is added to provide whiteness, opacity and UV protection [80]. Finally, Si is present in both the red and white paints, probably as SiO_2, to improve mechanical properties and/or to the silanes used in the primer coat [81]. SEM micrographs (BSE) at different magnifications together with composition maps of the red and white paints are available in supplementary material (Fig. S1).

3.2. Laser paint removal

3.2.1. Efficiency of paint removal

Laser ablation tests were conducted on a (10 × 10) mm^2 surface using parallel sweeps separated by a distance that ensured a clean zone. The tests were performed with the laser beam focused at the sample surface at normal incidence. Decisions on the most appropriate values for efficient paint removal (higher extraction) were made through a series of exploratory experiments, taking into paint removal were made through a series of exploratory experiments, taking into account previous studies on the removal of spray paint using ultrashort pulse lasers. The parameters involved in laser treatments, such as repetition frequency, fluence, scan speed, and laser trajectories, were considered [90].

The preliminary test results were evaluated through visual inspection using an optical microscope. The selected irradiation conditions for this study were those that produced a clean surface with no significant paint residue and no visible damage to the gel-coat. Therefore, the values used were: average power$P$ = 4 W; repetition frequency$f$ = 50 kHz; working distancew_d = 0; scan speed$v$ = 750 mm•s^{-1}; and line-to-line displacement of 15 μm. The applied fluence was 10 J•cm^{-2}. With these parameters, successive horizontal and vertical scans were performed until the treated area was free of paint.

Fig. 4 displays optical microscope images of the laser-treated areas as the number of laser passes increases. For the red-SP sample (Fig. 4a), the degree of paint removal is low after 2 passes, and a darkening of the remaining paint is visible. After 5 passes, the paint is entirely removed, and the intermediate primer layer (dark grey) becomes visible. At 6

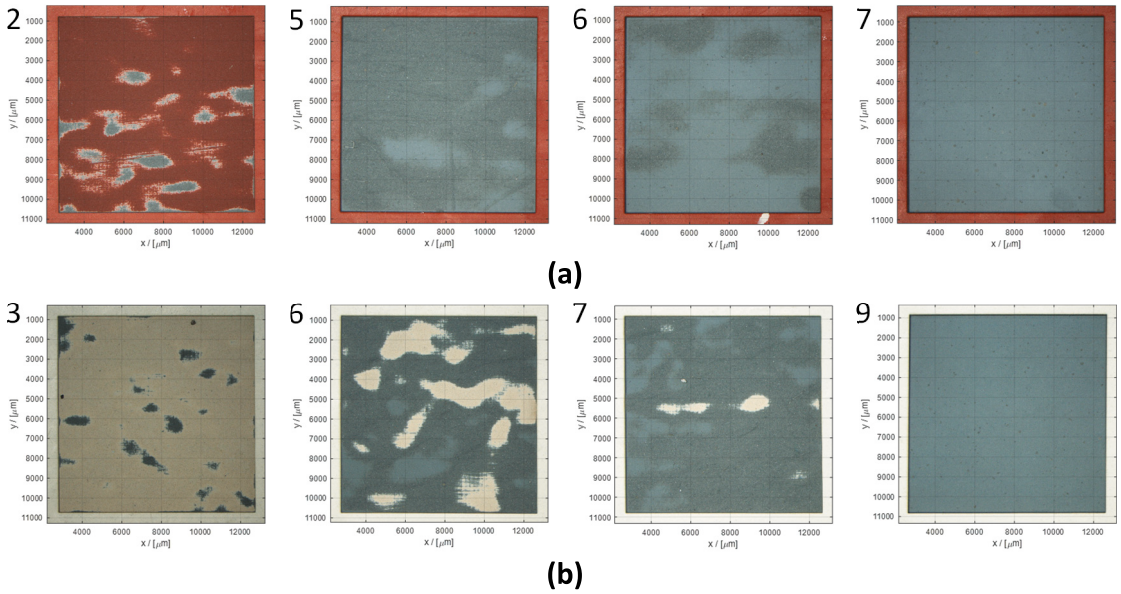

Fig. 4. Optical microscope images of the red-SP (a) and white-HM (b) samples after laser cleaning with increasing number of passes (indicated by the number in the box). (For interpretation of the references to color in this figure legend, the reader is referred to the web version of this article.)

passes, most of the substrate is clean (lighter areas). Finally, after 7 passes, the surface achieves a satisfactory level of cleanliness. At this microscope magnification, no traces of coating, paint or primer can be detected. The images of the white-HM sample (Fig. 4b) indicate a slower transition between the different layers. Therefore, after 3 passes, the degree of paint removal is low and the darkening of the antifouling paint is visible. After 6 passes, the substrate is still partially coated with antifouling paint, while most of it is covered by the primer film. By the 7th pass, the paint is almost completely removed, and the substrate is almost entirely covered by the primer film. After 9 passes, the paint is satisfactorily removed. It is important to note that achieving a total and uniform cleaning of the red and white painted surfaces required 7 and 9 passes, respectively. This was due to the non-uniformity of the layers.

To measure the ablation rate of both antifouling paints, we analysed the laser-generated cavities using microscope interferometry and measured their depth as the number of laser passes increased. Fig. 5 displays the topographic reconstruction of the well-defined structures in the red-SP (Fig. 5a) and white-HM (Fig. 5b) paints after 6 and 7 passes, respectively, as well as the cavity depth as a function of the number of laser passes for each sample (Fig. 5c). The data show that the ablation depth increases in a nearly linear manner with the number of laser passes. The slopes obtained from the linear fit indicate a lower ablation rate (17.87 $\mu m \cdot pass^{-1}$) for the hard matrix paint, white-HM, compared to the self-polishing, red-SP (21.76 $\mu m \cdot pass^{-1}$), which is expected due to the good mechanical resistance of the hard matrix antifouling. Both removal rate, expressed in $mm^3 \cdot min^{-1}$, and removal efficiencies expressed in $mm^3 \cdot (min \cdot W)^{-1}$, were also calculated and the results are shown in Table 2. The correlation coefficient R^2 of the fitted model is given in parentheses.

3.2.2. SEM-EDS and ATR analysis

SEM-EDS and FTIR-ATR were utilised to assess the effectiveness of the laser in removing the antifouling paints and to analyse the chemical composition of the gel-coat surface exposed after laser cleaning. The analysis focused on areas without paint and those with paint residues under the optical microscope. Specifically, for the red-SP sample, the areas treated with 2, 4, and 5 laser passes were examined, while for the white-HM sample, the areas treated with 3, 4, and 6 laser passes were analysed. Fig. 6 displays SEM images collected using the backscattered electron detector (BSE, 50x) alongside the composition maps for areas treated with 4 passes for the red SP sample (Fig. 6a, b) and 6 passes for the white-HM sample (Fig. 6d, e). The analysis focused on an area where the different layers (traces of paint, primer and gel-coat) were visible.

It can be seen from the micrographs that the composition of each layer is clearly distinguishable thanks to their particular textures; so that in the area with red antifouling paint (Fig. 6a), the markers are the high contrast grains composed of Cu (CuO_2) and Zn (ZnO). EDS elemental analysis indicated the presence of Cu (11.4 %), Zn (10.3 %), Si (1.7 %) and S (1.3 %) in this zone, as shown in the corresponding composition map (Fig. 6b). In the white antifouling zone (Fig. 6d), the markers are the high-contrast coarser grains composed of Cu and S (CuSCN), as well as the finer and evenly distributed particles of Zn (ZnO) and Ti (TiO_2), both with strong contrasts. EDS elemental analysis revealed the presence of Cu (4.4 %), S (2.5 %), Zn (9.2 %), Ti (9.0 %) and Si (1.3 %) (Fig. 6e). The results of the SEM-EDS analyses showed that the composition of the primer and gel-coat layers is the same for the red-SP and white-HM samples; therefore, they are described together (EDS spectra data correspond to the red-SP sample). With respect to the primer layer (Fig. 6a, d), the marker is Si in the form of large particles of intermediate contrast on the surface and Ti is also present in the form of small particles of high contrast. The spectrum collected in this area indicates that the primer contains Si (7.0 %), Ti (4.9 %) and Mg (3.5 %) as major elements and Fe (0.6 %) and Al (0.5 %) in smaller amounts (Fig. 6b, e). The presence of Si may be due to the silane coupling agents used to improve the adhesion on the substrate (gel-coat) [91]. Finally, the gel-coat zone (Fig. 6a, d) is distinguished by its dark contrast; the presence of high-contrast Ti particles is also observed in this layer. EDS analysis revealed that the dark contrast zone is due to C enrichment; in addition, Ti (9.2 %), Si (3.5 %), Mg (1.6 %) and Al (0.4 %) were detected (Fig. 6b, e).

By SEM-EDS, no traces of antifouling paints or primer were detected on the revealed gel-coat surface after laser treatment. Indeed, the gel-coat layer is easily identified by its low contrast in BSE mode and its C and Ti content in the micrographs corresponding to the red-SP (Fig. 6c) and white-HM (Fig. 6f) samples.

The spectra obtained by FTIR microscopy in the ATR mode for both red and white paints and the corresponding treated surfaces upon increasing laser passes are plotted in Fig. 7. The spectra of two different areas after 4 and 6 passes in Fig. 7a and b, respectively, have been included in order to show the heterogeneity of the surface at these stages

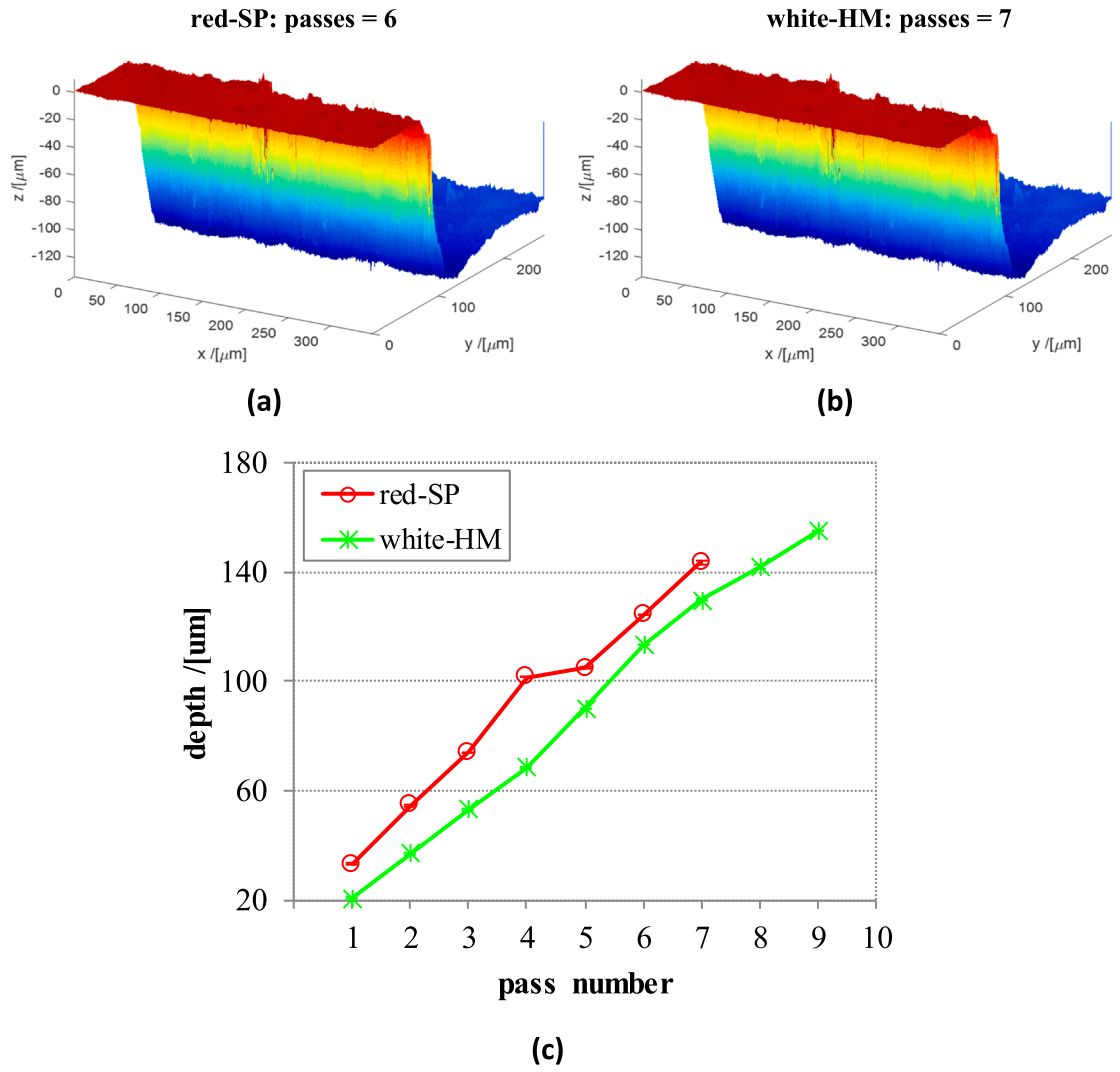

Fig. 5. Topographic reconstruction of the cavities created on the red-painted (a) and white-painted (b) samples at 6 and 7 passes, respectively. (c) Cavity depth as a function of the number of laser passes for each sample. (For interpretation of the references to color in this figure legend, the reader is referred to the web version of this article.)

Table 2
Depth per pass and R^2 (in parentheses), material removal rate and ablation efficiency for each sample.

Sample	Depth [μm pass^{-1}]	Removal rate [mm^3 min^{-1}]	Efficiency [mm^3 (min W)$^{-1}$]
red-SP	21.76 (0.93)	7.12	1.78
white-HM	17.87 (0.99)	5.84	1.46

of the cleaning process. The corresponding spectra are noted as 4.1, 4.2 passes and 6.1, 6.2 passes for the red-SP and white-HM samples, respectively.

In relation with the red-SP sample (Fig. 7a), increasing the number of laser passes leads to the progressive decrease of the bands assigned to the metal carboxylate complexes at around 1585–1540 cm^{-1} and 1390 cm^{-1}, asymmetric and symmetric stretching vibrations of the CO_2^- groups, respectively. These bands disappeared completely after 5 passes and in the most part of the treated surface after 4 passes (Fig. 7a, spectrum noted as 4.2). Additionally, the ATR conventional spectrum of a totally cleaned area (see Fig. S2 in supplementary data) showed the complete disappearance of the strong band at 604 cm^{-1} allotted to the Cu–O bond. These spectral alterations agree with the SEM-EDS elemental analyses which demonstrate the absence of Zn and Cu elements and therefore, the complete paint removal in the areas identified as primer and gel-coat. Concerning the white-HM sample (Fig. 7b), the most noticeable changes in the infrared spectra from the first laser passes are the progressive reduction of the band assigned to the thiocyanate at 2155 cm^{-1}, along with the bands attributed to the metal carboxylate complexes at around 1585–1540 cm^{-1} and 1390 cm^{-1} ($\upsilon_{\bar{C}OO}$ asymmetric and symmetric, respectively) until their complete disappearance in most spots after 6 passes (Fig. 7b, spectrum noted as 6.2 in contrast with spectrum 6.1, showing the SCN band indicative of paint residues) and on the cleaned surface. As well as in the red-SP sample, these spectral modifications support the results obtained by SEM-elemental analysis in the areas identified as primer and gel-coat, in which no Zn, Cu or S are detected, ratifying the efficiency of the cleaning treatment.

The rest of the spectral changes observed are very similar in the red-SP and white-HM samples, thus they are described together. Parallel to the disappearances of the aforementioned bands, the progressive appearance of new strong bands is detected. The most intense one is the broad band spanning from 1063 to 840 cm^{-1}, centered at 1000 cm^{-1} and with some shoulders in the lower frequency region. These features reveal the presence of several asymmetric Si-O-Si stretching modes

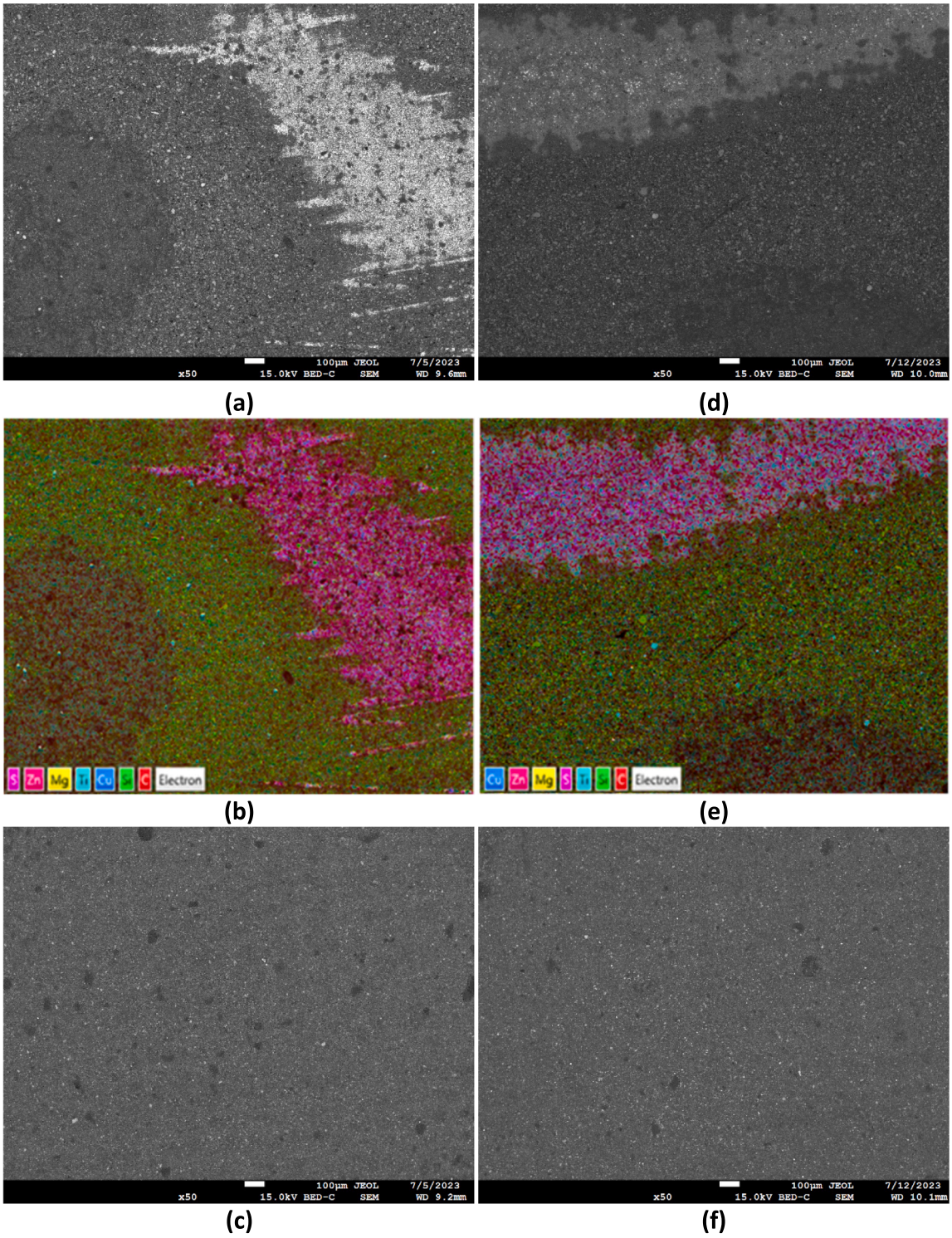

Fig. 6. SEM micrographs (BSE, 50x) together with composition maps of the surface after laser cleaning with different number of passes. (a-c) red-SP sample and (d-f) white-HM sample. (For interpretation of the references to color in this figure legend, the reader is referred to the web version of this article.)

[92,93]. Further, the new peaks centered at 1230 and 821 cm^{-1} can be assigned to the bending and rocking vibrations of Si-CH3 and Si-$(CH3)_2$ groups, respectively. Simultaneously, the increase of the broad band between 3600–3000 cm^{-1} (ν_{OH}) may be caused by the occurrence of –Si-OH groups. These bands can be mainly ascribed to the silicate filler (SiO2) and even to traces of the silanes in the primer [93]. Only in the red-SP sample and in some areas after 4 or 5 passes, the band assigned to the stretching of Ti-O bond at 727 cm^{-1} (clearly detected in the original gel-coat spectrum) reappears [80]. The changes just described, together with the results of SEM-EDS analysis, can be explained by the progressive exposure of the primer layer and gel-coat after paint removal.

Further, additional new bands are detected at around 1643 and 1506 cm^{-1} from 4 and 6 passes for the red-SP and white-HM samples, respectively. These bands are not present in the original gel-coat spectrum and their origin could be ascribed to the bending of OH groups from water molecules hydrogen bonded to the Si-O-Si structure, and to the appearance of negatively charged silane groups (−SiO-), respectively [92]. Another possible origin of these bands is the increasing

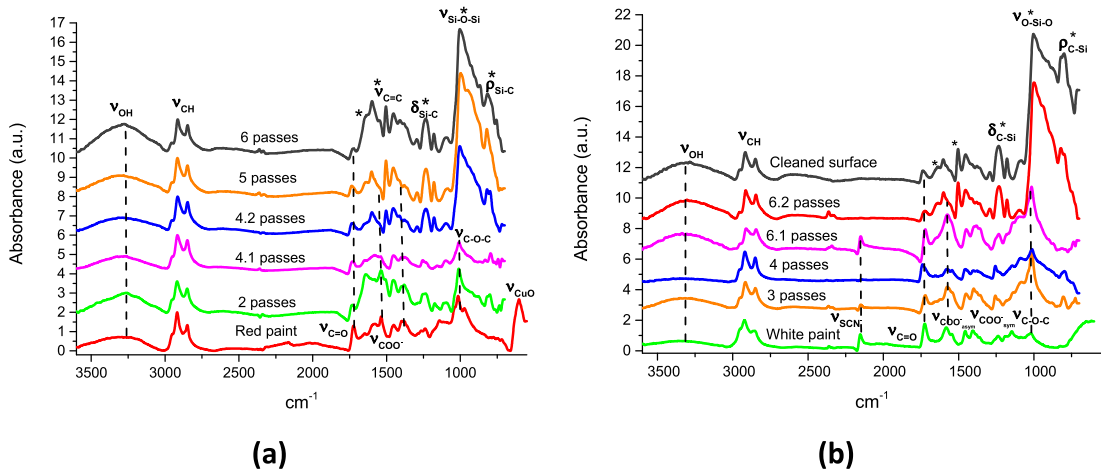

Fig. 7. Normalised ATR-FTIR spectra of the red-SP (a) and white-HM (b) samples before cleaning and laser treated areas upon increasing laser passes. (For interpretation of the references to color in this figure legend, the reader is referred to the web version of this article.)

presence of aromatic moieties, which together with the decrease in the carbonyl stretching band centered at 1723 cm^{-1}, may be due to the chemical degradation of the polyester resin produced by laser radiation [94,95]. The latter degradation reactions might explain the change in coloration to a greyer and darker appearance of the gel-coat after the laser treatment. Similar changes in coloration and increasing darkness have been described by previous authors in laser cleaning of spray paints [74,96]. Further, using optical microscopy and SEM of cross-sections of the laser-treated samples (see Fig. S3 in supplementary data), it was possible to estimate the thickness of the altered gel-coat layer to be about 10 − 15 μm i.e. the laser alteration effects are confined to the outermost layers of the gel-coat and do not affect the polymer bulk.

3.3. Surface morphology characterization

The morphology of the laser cleaned surfaces was observed by both electron microscopy and interferometric microscopy.

SEM images in secondary electron mode of the surfaces before and after laser cleaning are shown in Fig. 8. Areas with residues of paint were also analyzed, the corresponding micrographs are provided in supplementary material (Fig. S4). As can be seen, superimposed to the laser generated crosshacht pattern, small bumps appear, not noticeable in BSE mode, and the surfaces become rough after processing of both red-SP (Fig. 8a, b) and white-HM (Fig. 8a, d) samples. It can be observed that the femtosecond pulses generated a micrometer-scale (<10 μm) a granulate or globularpattern on the surfaces (Fig. 8c, e).

Interferometric microscopy corroborates the SEM observations as can be seen in Fig. 9 where topographies of the pristine gel-coat surface (Fig. 9a) and the laser-treated surfaces (Fig. 9b, c) are shown. As can be seen, the resulting surface is rougher after laser cleaning. As mentioned previously, surface roughness could play a crucial role in the repainting procedure, owing to the fact that suitable roughness favours the bonding performance between coatings.

Roughness is typically characterised by the mean roughness S_a and root mean square roughness S_q. However, these amplitude parameters alone are insufficient to describe the complexity of the surface. Therefore, this work includes parameters that evaluate the shape of the height distribution, namely the skewness S_{sk} and the kurtosis S_{ku}. In addition, we have included the developed interfacial area ratio S_{dr}, which is a significant parameter for surface wettability. Table 3 depicts the values of these areal roughness parameters, measured before and after laser treatment, in addition with those of the mechanically cleaned surface. It can be seen that both S_a and S_q of the laser cleaned surface are about twice the values of the untreated gel-coat. As for the parameters evaluating the shape of the height distribution, the skewness S_{sk}, is around zero; which results congruent with the applied laser scanning scheme (crosshatch) and the kurtosis S_{ku}, around 3, indicating a more homogeneous height distribution and less pronounced surface peaks after laser processing compared to the untreated gel-coat surface (reference surface). With respect to the gel-coat after conventional mechanical paint removing, S_a and S_q also increase, but unlike the laser treatment in this case the distribution of heights is no longer symmetrical, with a negative skewness S_{sk} and a kurtosis S_{ku} above 3; which indicates the presence of sharp peaks.

The developed interfacial area ratio, S_{dr} expressed as the percentage of the definition area's additional surface area contributed by the texture as compared to the planar definition, experiments an important increase with respect to the untreated gel-coat after laser paints removal, so that $S_{dr} = 0.10 \pm 0.01$ in the pristine gel-coat and$S_{dr} = 0.78 \pm 0.00$ and$S_{dr} = 0.68 \pm 0.01$ for removed red-SP and white-HM, respectively. On the other hand, after mechanical cleaning, the resulting gel-coat surfaces are more irregular (Fig. 9d, e) and with lower values of S_a and S_q than the laser-treated ones, and consequently the developed area S_{dr} is lower; resulting$S_{dr} = 0.38$ for both red-SP and white-HM cleaned samples.

3.4. Wettability evaluation

The behaviour of solid surfaces in a wide range of applications depends on the wetting response; so that it is important to evaluate how the surface modifications in the gel-coat layer after femtosecond laser paint removal affects its wetting characteristics. The wettability is usually characterised in terms of the static contact angle, θ, that describes the behaviour of a liquid droplet on a solid surface in air, and is defined as the angle between the tangent at the three-phase point and the solid surface. Solid surfaces with $\theta < 90^{\circ}$ are considered hydrophilic, while surfaces with $\theta \geq 90^{\circ}$ are considered hydrophobic. Fig. 10 shows the contact angle values of the antifouling painted surfaces and the gel-coat, obtained both for the pristine sample and for the samples cleaned by the laser and mechanical methods; the contact angle values have been calculated with 95 % confidence. As can be observed, the self-polishing coating (red-SP) with $\theta = 92.8^{\circ} \pm 0.1^{\circ}$ shows hydrophobic behaviour ($\theta > 90^{\circ}$) while the hard matrix one (white-HM) with $\theta = 78.3^{\circ} \pm 0.5^{\circ}$ has hydrophilic character ($\theta < 90^{\circ}$), in agreement with other reported results [97].

With respect to the uncoated gel-coat surface (reference surface), the contact angle is $\theta = 79.2^{\circ} \pm 0.2^{\circ}$, corresponding to a hydrophilic character. After laser paint removal, the contact angle of the gel-coat increases to $\theta = 112.7^{\circ} \pm 0.3^{\circ}$ (red-SP) and $\theta = 112.2^{\circ} \pm 0.2^{\circ}$ (white-HM), so that the fs laser treated surface acquires a hydrophobic behaviour. In

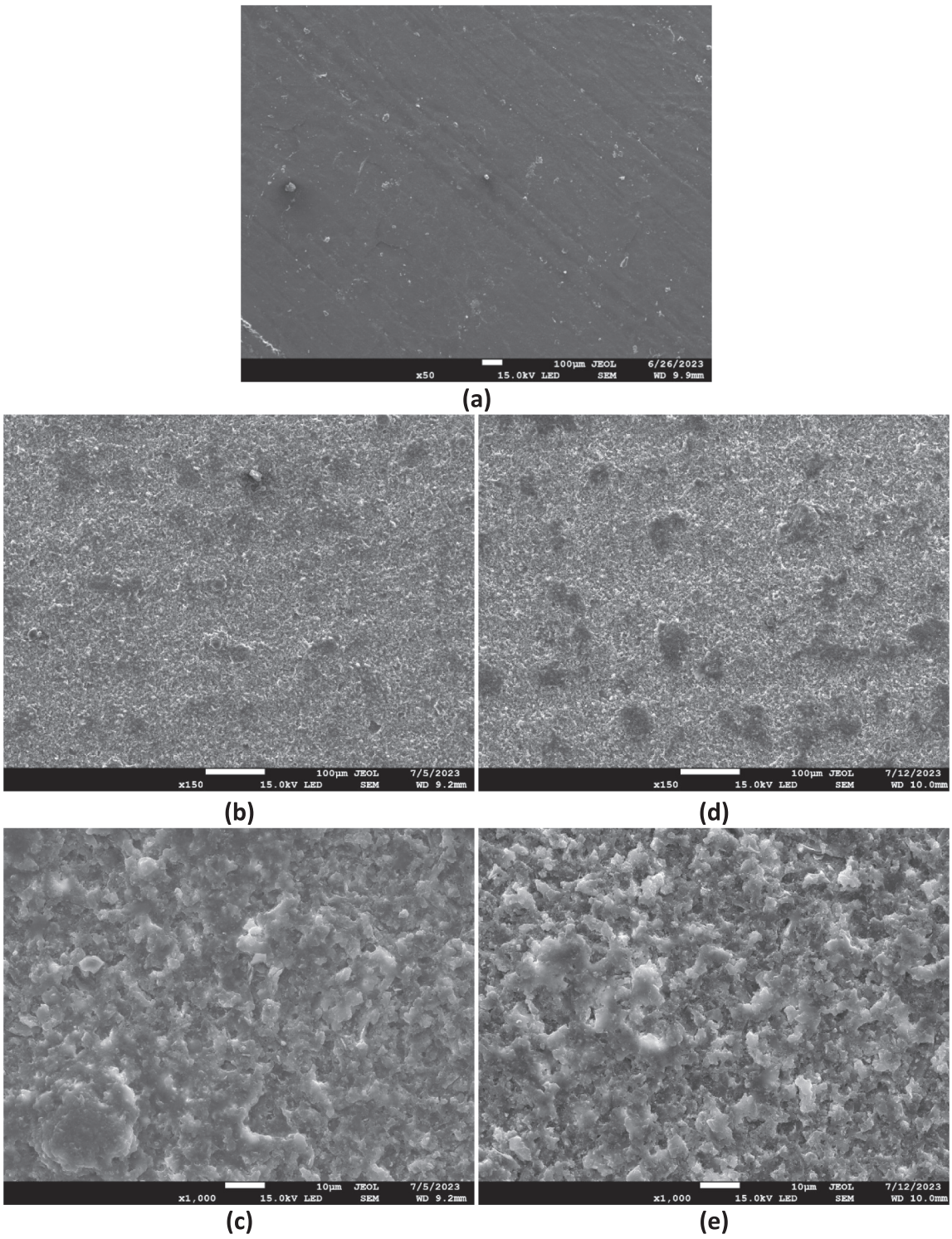

Fig. 8. SEM micrographs (SE) at different magnifications of surfaces before and after laser cleaning. (a) untreated gel-coat; (b, c) red-SP sample and (d, e) white-HM sample.

the case of the abraded surfaces, the contact angle also increases, although to slightly lower values than for the laser method, being $\theta = 111.1^\circ \pm 0.6^\circ$ for the red SP and $\theta = 109.7^\circ \pm 0.4^\circ$ for the white-HM. The greater dispersion of these values compared to those obtained with the laser method is due to the lower uniformity of the surface finish obtained with the mechanical method, as mentioned above, which makes the measurement more difficult.

Thus, despite the significant increase in gel-coat surface roughness after the femtosecond laser process, the wettability of the surface decreases; the same is observed when applying the conventional mechanical technique.

The wettability of a surface depends on its chemical composition and morphology. The changes in chemical composition observed by FTIR indicate a partial degradation of the gel-coat polyester resin with an increase in aromatic moieties, which could enhance hydrophobicity [94]. Although to a lesser extent than changes in surface roughness, these chemical modifications could contribute to the transition from a hydrophilic to a hydrophobic surface. Due to the greater importance of

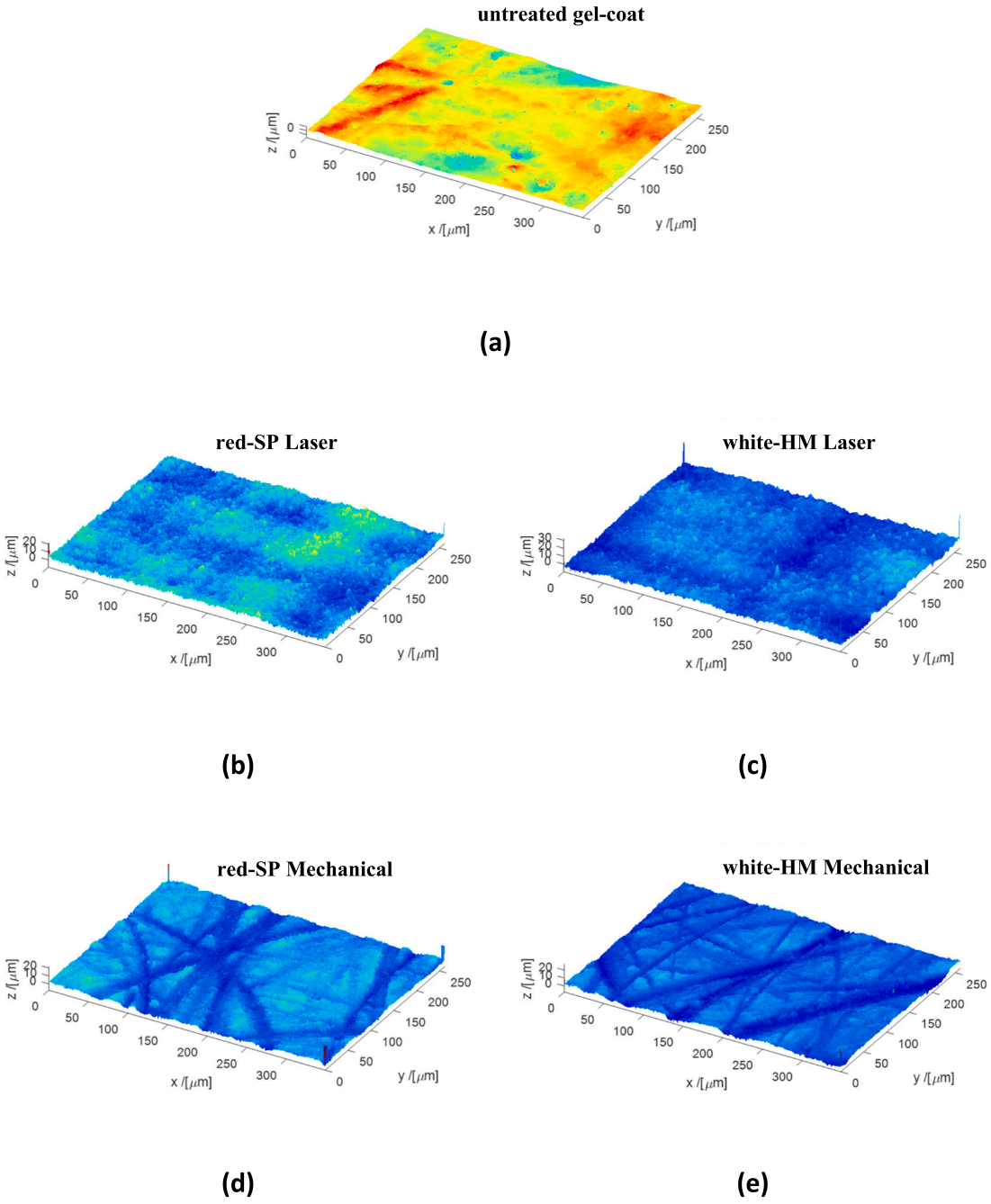

Fig. 9. Reconstruction of the surface topography of the samples before and after laser and mechanical cleaning: (a) untreated gel-coat; (b, c) laser cleaned red-SP and white-HM samples and (d, e) mechanically cleaned red-SP and white-HM samples. (For interpretation of the references to color in this figure legend, the reader is referred to the web version of this article.)

roughness, the study focuses on this property in the following paragraphs.

To explain the effect of surface roughness induced by the femtosecond laser on wettability, we must consider the S_{dr} parameter. This parameter is the roughness parameter that best approximates the increase in solid surface area in both the Wenzel and Cassie-Baxter wettability models [98]. The Wenzel theory implies that a hydrophilic surface ($\theta_0 < 90^\circ$) will become more hydrophilic as the surface roughness increases. The Wenzel contact angle (θ_W) varies according to the equation, equation (Eq. (1))

$$\cos\theta_W = r\cos\theta_0 \tag{1}$$

where the roughness ratio r is defined as the ratio of the actual surface area wetted by the liquid and the projected planar area ($r = 1 + S_{dr}$). Wenzel equation is based on the hypothesis that liquid enters irregularities present on the surface, leading to a homogeneous wetting regime with an increased contact area [99]. In the wetting regime given by the Cassie-Baxter model (Eq. (2)), it is energetically favourable for the liquid to form a droplet that rests on the edges of the surface while air fills the space between solid and liquid, forming air pockets [99]. Consequently,

Table 3
S_a (arithmetic mean value), S_q (root mean square roughness), S_{sk} (skewness), S_{ku} (kurtosis) and S_{dr} (developed interfacial area ratio) for untreated and cleaned samples.

	S_a[μm]	S_q[μm]	S_{sk}	S_{ku}	S_{dr}
UNTREATED SURFACES					
red-SP	0.70 ± 0.18	0.87 ± 0.22	0.19 ± 0.32	3.48 ± 0.62	0.08 ± 0.01
white-HM	0.91 ± 0.15	1.15 ± 0.22	0.28 ± 0.30	3.37 ± 0.34	0.13 ± 0.03
gel-coat	1.01 ± 0.15	1.31 ± 0.20	−0.12 ± 0.27	3.85 ± 0.58	0.10 ± 0.01
LASER CLEANING					
red-SP	2.05 ± 0.30	2.55 ± 0.38	0.01 ± 0.19	2.91 ± 0.01	0.78 ± 0.00
white-HM	1.92 ± 0.25	2.38 ± 0.29	−0.09 ± 0.01	2.88 ± 0.15	0.68 ± 0.01
MECHANICAL CLEANING					
red-SP	1.51 ± 0.10	1.82 ± 0.13	−0.41 ± 0.08	3.59 ± 0.17	0.38 ± 0.02
white-HM	1.37 ± 0.09	1.74 ± 0.09	−0.50 ± 0.11	3.62 ± 0.48	0.38 ± 0.01

only a small fraction of the solid surface is in contact with the liquid. The Cassie-Baxter contact angle θ_{CB} can be calculated as:

$$\cos\theta_{CB} = -1 + f + r_f f \cos\theta_0$$

or

$$\cos\theta_{CB} = r_f \cos\theta_0 - f_G\left(r_f \cos\theta_0 + 1\right) \quad (2)$$

where f is the fraction of the projected area of the solid surface under the drop that is wetted by the liquid (solid–liquid fraction), f_G is the liquid–air fraction ($f + f_G = 1$) and r_f is the roughness ratio of the wetted area. When $f = 1$, $r_f = r$ and the Cassie-Baxter equation is equivalent to the Wenzel equation. It is important to note that both equations are correct only if the drop is sufficiently large in relation to the typical roughness scale [100].

In this theoretical framework, the Cassie-Baxter model would explain the behaviour of the gel- coat surface observed after the application of laser and mechanical cleaning methods. By increasing the liquid–air fraction f_G, an initially hydrophilic surface can become hydrophobic [101]. For this change in surface behaviour to take place, f_G must have a minimum value and, in addition, it must be higher the rougher the surface is (increase of r_f) [102].

In previous work on femtosecond laser texturing [103,104] we have found that the morphology and scale of roughness are influenced by a variety of parameters, of which material properties and laser parameters are the most important. Thus, for a given material, it might be possible to modify its surface morphology to tailor its wettability by selecting the appropriate laser processing parameters. However, in this work we have focused on analysing the feasibility of the fs laser for the removal of antifouling paints on a polymeric material, choosing the process parameters according to complete paint removal and minimal thermal damage to the substrate gel-coat. Based on the results obtained, further analysis of the irradiation parameters would be required to explore the possibility of selectively roughening the gel-coat substrate to increase its wettability.

4. Conclusions

In this paper we present what we consider to be, to the best of our knowledge, a novel femtosecond laser cleaning method for the removal of surface coatings of antifouling paints on GFRP laminates used in maritime applications. The paints used in this study correspond to the most common types in this field, referred to as hard matrix and self-polishing antifouling paints, respectively. Prior to laser cleaning, the paints and the GFRP surface were characterised and the efficiency of the laser ablation process was evaluated in terms of paint removal and effects on the polymer substrate. The results were compared with those obtained by the conventional mechanical method. The main conclusions of this study are as follows:

- Characterisation of the different layers of the samples, i.e. gel-coat, primer and antifouling paints was first carried by FTIR and SEM-EDS. The gel-coat consists of an aromatic polyester resin, plus a relatively high content of TiO_2 and SiO_2 added as fillers. Both antifouling paints comprise a similar acrylic binder plus biocides and other inorganic fillers. Especifically, the synergistic combination of the biocides Cu_2O and ZnO was proved in the red-SP, whereas Copper(I) thiocyanate and ZnO have been detected in the white-HM. The hard matrix paint further contains a relatively high amount of TiO_2. Lastly, Si (around 1 %) was identified in both antifouling paints and assigned to SiO_2 and/or to the silanes used in the primer coat.
- The femtosecond pulsed laser can effectively clean the multi-layer coating on the top surface of the GFRP with minimal thermal effects on the GFRP substrate by selecting the appropriate process parameters. Complementary analyses by optical microscopy, SEM-EDS and FTIR performed after successive passes of the laser, allowed us to evaluate the effectiveness of the treatment. The

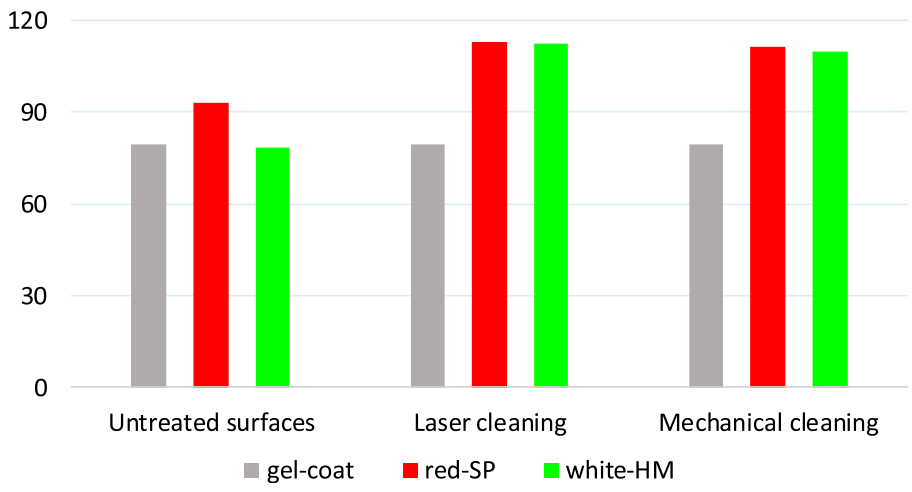

Fig. 10. Contact angle θ [°] for untreated and cleaned samples (reference surface contact angle has been repeated for easy reading).

complete paint removal was achieved after 7 passes and 9 passes on the red-SP and white-HM samples, respectively.

- The ablation rate values obtained for both coatings demonstrate the feasibility of the fs laser to remove, layer by layer, a typical coating thickness of about 100 μm. In this sense, an ablation rate of 17.87 μm·pass^{-1} was obtained for the hard matrix antifouling paint and 21.76 μm·pass^{-1} for the self-polishing paint.
- Chemical changes have been detected in the gel-coat after laser treatment. The darkening of the gel-coat is parallel to the variation in the elemental composition (enrichment in C, decrease in TiO_2) and the appearance of new bands in the FTIR spectrum (assigned to aromatic groups due to partial degradation of the polyester resin). Nevertheless, the alteration effects are limited to the outermost layers of the gel-coat (10–15 μm) and do not affect the mass of the polymer bulk.
- The morphology of the gel-coat surface after laser cleaning changes and becomes rougher, with mean roughness values almost double those of the uncoated gel-coat and also higher than those obtained by the conventional mechanical method. In addition, the surface texture produced by the fs laser has a regular pattern, with a more homogeneous height distribution and less pronounced surface peaks than the mechanically treated surface. In addition, the fs laser gives a significant increase in the developed area S_{dr}.
- The untreated gel-coat surface has a hydrophilic character with a contact angle of 79.2°. The laser treatment results in an increase in the initial contact angle to a value of approximately 112°; which corresponds to the Casie-Baxter wettability model. Similar results were obtained for the mechanically cleaned surfaces.

In conclusion, this work demonstrates the validity and efficiency of the femtosecond laser cleaning method for paint removal on GFRP with minimal thermal damage to the substrate. Furthermore, given that the surface roughness can be controlled by tuning the laser parameters, further work is required to optimise the irradiation parameters to remove the paint and produce a texture that increases the wettability of the surface.

CRediT authorship contribution statement

Alicia Moreno-Madariaga: Writing – original draft, Methodology, Investigation, Formal analysis, Data curation, Conceptualization. **Aurora Lasagabáster-Latorre:** Writing – original draft, Resources, Investigation, Formal analysis. **María L. Sánchez Simón:** Resources, Investigation. **Javier Lamas:** Resources, Investigation, Formal analysis, Conceptualization. **Alberto Ramil:** Supervision, Software, Methodology, Investigation, Formal analysis, Conceptualization. **Ana J. López:** Writing – review & editing, Supervision, Project administration, Methodology, Funding acquisition, Formal analysis, Conceptualization.

Declaration of competing interest

The authors declare that they have no known competing financial interests or personal relationships that could have appeared to influence the work reported in this paper.

Data availability

Data will be made available on request.

Funding and Acknowledgements

This research was partially supported by Grant PID2021-123948OB-I00 funded by MCIN/AEI/10.13039/501100011033 and by “ERDF A way of making Europe”, by the “European Union”.

Appendix A. Supplementary data

Supplementary data to this article can be found online at https://doi.org/10.1016/j.optlastec.2024.111479.

References

[1] F. Rubino, A. Nisticò, F. Tucci, P. Carlone, Marine Application of Fiber Reinforced Composites: A Review, Journal of Marine Science and Engineering 8 (1) (2020) 26, https://doi.org/10.3390/jmse8010026.
[2] C. Scianni, E. Georgiades, Vessel In-Water Cleaning or Treatment: Identification of Environmental Risks and Science Needs for Evidence-Based Decision Making, Front. Mar. Sci. 6 (2019) 467, https://doi.org/10.3389/fmars.2019.00467.
[3] A. Carchen, M. Atlar, Four KPIs for the assessment of biofouling effect on ship performance, Ocean Eng. 217 (2020) 107971, https://doi.org/10.1016/j.oceaneng.2020.107971.
[4] M.P. Schultz, J.A. Bendick, E.R. Holm, W.M. Hertel, Economic impact of biofouling on a naval surface ship, Biofouling 27 (1) (2011) 87–98, https://doi.org/10.1080/08927014.2010.542809.
[5] R. Adland, P. Cariou, H. Jia, F.-C. Wolff, The energy efficiency effects of periodic ship hull cleaning, J. Clean. Prod. 178 (2018) 1–13, https://doi.org/10.1016/j.jclepro.2017.12.247.
[6] I. Davidson, C. Scianni, C. Hewitt, R. Everett, E. Holm, M. Tamburri, G. Ruiz, Mini-review: Assessing the drivers of ship biofouling management – aligning industry and biosecurity goals, Biofouling 32 (4) (2016) 411–428, https://doi.org/10.1080/08927014.2016.1149572.
[7] B. Hyun, P.-G. Jang, M.-C. Jang, J.-H. Kang, J.-H. Kim, J.-S. Ki, D.H. Choi, O. H. Yu, J.-Y. Seo, W.-J. Lee, K. Shin, Development of Biological Risk Assessment Protocols for Evaluating the Risks of In-Water Cleaning of Hull-Fouling Organisms, Journal of Marine Science and Engineering 12 (2) (2024) 234, https://doi.org/10.3390/jmse12020234.
[8] Z.Y. Soon, J.-H. Jung, C. Yoon, J.-H. Kang, M. Kim, Characterization of hazards and environmental risks of wastewater effluents from ship hull cleaning by hydroblasting, J. Hazard. Mater. 403 (2021) 123708, https://doi.org/10.1016/j.jhazmat.2020.123708.
[9] A. Turner, Marine pollution from antifouling paint particles, Mar. Pollut. Bull. 60 (2) (2010) 159–171, https://doi.org/10.1016/j.marpolbul.2009.12.004.
[10] A. Turner, Metal contamination of soils, sediments and dusts in the vicinity of marine leisure boat maintenance facilities, J. Soil. Sediment. 13 (6) (2013) 1052–1056, https://doi.org/10.1007/s11368-013-0686-2.
[11] M. Carve, A. Scardino, J. Shimeta, Effects of surface texture and interrelated properties on marine biofouling: a systematic review, Biofouling 35 (6) (2019) 597–617, https://doi.org/10.1080/08927014.2019.1636036.
[12] C.M. Magin, S.P. Cooper, A.B. Brennan, Non-toxic antifouling strategies, Mater. Today 13 (4) (2010) 36–44, https://doi.org/10.1016/S1369-7021(10)70058-4.
[13] E.R. Silva, O. Ferreira, P.A. Ramalho, N.F. Azevedo, R. Bayón, A. Igartua, J. C. Bordado, M.J. Calhorda, Eco-friendly non-biocide-release coatings for marine biofouling prevention, Sci. Total Environ. 650 (2019) 2499–2511, https://doi.org/10.1016/j.scitotenv.2018.10.010.
[14] J. Telegdi, L. Trif, L. Románszki, Smart anti-biofouling composite coatings for naval applications, in: Smart Composite Coatings and Membranes: Transport, Structural, Environmental and Energy Applications, Elsevier Inc., 2016, pp. 123–155, https://doi.org/10.1016/B978-1-78242-283-9.00005-1.
[15] J. Liang, Z. Wang, J. Gao, K. Gao, Path planning algorithm for laser removal of paint from aircraft skin, J. Coat. Technol. Res. 21 (2) (2024) 537–546, https://doi.org/10.1007/s11998-023-00836-w.
[16] S. Marimuthu, H.K. Sezer, A.M. Kamara, Applications of Laser Cleaning Process in High Value Manufacturing Industries, Developments in Surface Contamination and Cleaning: Applications of Cleaning Techniques 11 (2019) 251–288, https://doi.org/10.1016/B978-0-12-815577-6.00007-4.
[17] M.K.A.A. Razab, A. Mohamed Noor, M. Suhaimi Jaafar, N.H. Abdullah, F. M. Suhaimi, M. Mohamed, N. Adam, A.N. Yusuf, N. a., A review of incorporating Nd:YAG laser cleaning principal in automotive industry, J. Radiat. Res. Appl. Sci. 11 (4) (2018) 393–402, https://doi.org/10.1016/j.jrras.2018.08.002.
[18] G. Zhu, Z. Xu, Y. Jin, X. Chen, L. Yang, J. Xu, D. Shan, Y. Chen, B. Guo, Mechanism and application of laser cleaning: A review, Opt. Lasers Eng. 157 (2022) 107130, https://doi.org/10.1016/j.optlaseng.2022.107130.
[19] Z. Zhou, W. Sun, J. Wu, H. Chen, F. Zhang, S. Wang, The Fundamental Mechanisms of Laser Cleaning Technology and Its Typical Applications in Industry, Processes 11 (5) (2023) 1445, https://doi.org/10.3390/pr11051445.
[20] A. Kumar, M. Prasad, R.B. Bhatt, P.G. Behere, M. Afzal, A. Kumar, J.P. Nilaya, D. J. Biswas, Laser shock cleaning of radioactive particulates from glass surface, Opt. Lasers Eng. 57 (2014) 114–120, https://doi.org/10.1016/J.OPTLASENG.2014.01.013.
[21] M. Nevins, M. Nevins, A. Yamamoto, T. Yoshino, Y. Ono, C.-W. Wang, D. Kim, Use of Er:YAG Laser to Decontaminate Infected Dental Implant Surface in Preparation for Reestablishment of Bone-to-Implant Contact, Int J Periodontics Restorative Dent 34 (4) (2014) 461–466, https://doi.org/10.11607/prd.2192.
[22] M.P. Fiorucci, A.J. López, A. Ramil, S. Pozo, T. Rivas, Optimization of graffiti removal on natural stone by means of high repetition rate UV laser, Appl. Surf. Sci. 278 (2013) 268–272, https://doi.org/10.1016/j.apsusc.2012.10.092.
[23] P. Pouli, M. Oujja, M. Castillejo, Practical issues in laser cleaning of stone and painted artefacts: Optimisation procedures and side effects, Appl. Phys. A Mater.

Sci. Process. 106 (2) (2012) 447–464, https://doi.org/10.1007/s00339-011-6696-2.
[24] T. Rivas, S. Pozo, M.P. Fiorucci, A.J. López, A. Ramil, Nd:YVO4 laser removal of graffiti from granite. Influence of paint and rock properties on cleaning efficacy, Appl. Surf. Sci. 263 (2012) 563–572, https://doi.org/10.1016/j.apsusc.2012.09.110.
[25] S. Siano, J. Agresti, I. Cacciari, D. Ciofini, M. Mascalchi, I. Osticioli, A. A. Mencaglia, Laser cleaning in conservation of stone, metal, and painted artifacts: State of the art and new insights on the use of the Nd:YAG lasers, Appl. Phys. A Mater. Sci. Process. 106 (2) (2012) 419–446, https://doi.org/10.1007/S00339-011-6690-8/FIGURES/34.
[26] W.M. Steen, J. Mazumder, Laser Cleaning, in: Laser Material Processing, Springer, London, 2010, pp. 417–440, https://doi.org/10.1007/978-1-84996-062-5_11.
[27] T. Kaster, J.-H. Rissom, L. Gorissen, P. Walderich, J.-N. Schneider, C. Hinke, Approach toward the application of mobile robots in laser materials processing, J. Laser Appl. 35 (4) (2023) 042015, https://doi.org/10.2351/7.0001127.
[28] H.C. Lee, N.E. Pacheco, L. Fichera, S. Russo, When the End Effector Is a Laser: A Review of Robotics in Laser Surgery, Advanced Intelligent Systems 4 (10) (2022) 2200130, https://doi.org/10.1002/aisy.202200130.
[29] Z. Pan, D. Liu, S. Li, Z. Deng, J. Liu, T. Chen, Path planning and pose correction of robot laser cleaning process for specific surfaces of parts, Int. J. Adv. Manuf. Technol. 127 (1–2) (2023) 349–364, https://doi.org/10.1007/s00170-023-11535-6.
[30] Rodríguez, A., López, A. J., Lamas, J., Moreno, A., & Ramil, A. (2021). Development of a laser cleaning robot system for the processing of 3D surfaces. In S. Negahdaripour, E. Stella, D. Ceglarek, & C. Möller (Eds.), Multimodal Sensing and Artificial Intelligence: Technologies and Applications II (p. 28). SPIE. 10.1117/12.2592111.
[31] A. Rodríguez, A.J. López, J. Lamas, A. Moreno, A. Ramil, Robot-assisted laser ablation for 3D surfaces. Application for paint removal with ultrashort pulse laser, Opt. Lasers Eng. 160 (2023) 107284, https://doi.org/10.1016/j.optlaseng.2022.107284.
[32] J. Shuo, R. Yuan, M. Qingzeng, G. Hailong, L. Wenlong, C. Wei, Off-line programming of robot on laser cleaning for large complex components, J. Phys. Conf. Ser. 1748 (2) (2021) 022027, https://doi.org/10.1088/1742-6596/1748/2/022027.
[33] R. Delmdahl, J. Brune, R. Pätzel, Ultraviolet Laser Cleaning of Carbon Fiber Composites, Powder Metall. Met. Ceram. 55 (1–2) (2016) 1–4, https://doi.org/10.1007/s11106-016-9772-5.
[34] G. Greifzu, T. Kahl, M. Herrmann, W. Lippmann, A. Hurtado, Laser-based decontamination of metal surfaces, Opt. Laser Technol. 117 (2019) 293–298, https://doi.org/10.1016/J.OPTLASTEC.2019.04.037.
[35] S. Harder, H. Schmutzler, P. Hergoss, J. Freese, J. Holtmannspötter, B. Fiedler, Effect of infrared laser surface treatment on the morphology and adhesive properties of scarfed CFRP surfaces, Compos. A Appl. Sci. Manuf. 121 (2019) 299–307, https://doi.org/10.1016/j.compositesa.2019.02.025.
[36] H.A. Jasim, A.G. Demir, B. Previtali, Z.A. Taha, Process development and monitoring in stripping of a highly transparent polymeric paint with ns-pulsed fiber laser, Opt. Laser Technol. 93 (2017) 60–66, https://doi.org/10.1016/J.OPTLASTEC.2017.01.031.
[37] T. Shan, F. Yin, S. Wang, Y. Qiao, P. Liu, Surface integrity control of laser cleaning of an aluminum alloy surface paint layer, Appl. Opt. 59 (30) (2020) 9313, https://doi.org/10.1364/AO.404030.
[38] Q. Sun, J. Zhou, X. Meng, P. Li, Mechanical properties and microstructure characteristics of 2024–T351 aluminum alloy specimen subjected to paint removal by laser cleaning, Vacuum 211 (2023) 111927, https://doi.org/10.1016/j.vacuum.2023.111927.
[39] T.L. See, Z. Liu, S. Cheetham, S. Dilworth, L. Li, Laser abrading of carbon fibre reinforced composite for improving paint adhesion, Appl. Phys. A 117 (3) (2014) 1045–1054, https://doi.org/10.1007/s00339-014-8527-8.
[40] Y. Song, S. Wang, Y. Pan, Z. Li, L. Yu, Current research status of laser cleaning of carbon fiber reinforced polymers, Mater. Today Commun. 39 (2024) 109312, https://doi.org/10.1016/j.mtcomm.2024.109312.
[41] Z. Wang, Y. Ma, B. Yuan, C. Wu, C. Li, S. Sun, Development of Laser Processing Carbon-Fiber-Reinforced Plastic, Sensors 23 (7) (2023) 3659, https://doi.org/10.3390/s23073659.
[42] L. Hou, F. Yin, S. Wang, J. Sun, H. Yin, A review of thermal effects and substrate damage control in laser cleaning, Opt. Laser Technol. 174 (2024) 110613, https://doi.org/10.1016/j.optlastec.2024.110613.
[43] A.A. Cenna, P. Mathew, Evaluation of cut quality of fibre-reinforced plastics—A review, Int J Mach Tool Manu 37 (6) (1997) 723–736, https://doi.org/10.1016/S0890-6955(96)00085-5.
[44] J. Gu, X. Su, W. Li, Y. Jin, J. Xu, B. Guo, Process and mechanism of paint stripping on CFRP by UV nanosecond laser, Opt. Laser Technol. 171 (2024) 110461, https://doi.org/10.1016/j.optlastec.2023.110461.
[45] Y. Lu, L. Yang, M. Wang, Y. Wang, Improved thermal stress model and its application in ultraviolet nanosecond laser cleaning of paint, Appl. Opt. 59 (25) (2020) 7652, https://doi.org/10.1364/AO.398101.
[46] Z. Zhao, X. Liu, J. Yang, W. Pan, Y. Li, F. Liang, Y. Tian, L. Liu, F. Song, Shape evolution and characteristics of carbon fiber reinforced polymer surface in laser ablation, Vacuum 217 (2023) 112572, https://doi.org/10.1016/j.vacuum.2023.112572.
[47] Gamaly, E. (2011). Femtosecond laser-matter interaction: Theory, experiments and applications (1st ed.). Jenny Standford Publishing. 10.1201/9789814267809.
[48] J. Brand, A.V. Rode, S. Madden, A. Wain, P.L. King, L. Rapp, Ultrashort pulsed laser ablation of granite for stone conservation, Opt. Laser Technol. 151 (2022) 108057, https://doi.org/10.1016/J.OPTLASTEC.2022.108057.
[49] J. Brand, A. Wain, A.V. Rode, S. Madden, L. Rapp, Towards safe and effective femtosecond laser cleaning for the preservation of historic monuments, Appl. Phys. A 129 (4) (2023) 246, https://doi.org/10.1007/s00339-023-06455-x.
[50] M. Kono, K.G.H. Baldwin, A. Wain, A. Rode, v., Treating the untreatable in art and heritage materials: Ultrafast laser cleaning of “cloth-of-Gold”, Langmuir 31 (4) (2015) 1596–1604, https://doi.org/10.1021/LA504400H.
[51] T. Rivas, A.J. Lopez, A. Ramil, S. Pozo, M.P. Fiorucci, M.E.L. de Silanes, A. García, J.R.V. de Aldana, C. Romero, P. Moreno, Comparative study of ornamental granite cleaning using femtosecond and nanosecond pulsed lasers, Appl. Surf. Sci. 278 (2013) 226–233, https://doi.org/10.1016/j.apsusc.2012.12.038.
[52] M. Walczak, M. Oujja, L. Crespo-Arcá, A. García, C. Méndez, P. Moreno, C. Domingo, M. Castillejo, Evaluation of femtosecond laser pulse irradiation of ancient parchment, Appl. Surf. Sci. 255 (5 PART 2) (2008) 3179–3183, https://doi.org/10.1016/j.apsusc.2008.09.011.
[53] V. Oliveira, S.P. Sharma, M.F.S.F. de Moura, R.D.F. Moreira, R. Vilar, Surface treatment of CFRP composites using femtosecond laser radiation, Opt. Lasers Eng. 94 (2017) 37–43, https://doi.org/10.1016/j.optlaseng.2017.02.011.
[54] F.L. Palmieri, R.I. Ledesma, J.G. Dennie, T.J. Kramer, Y. Lin, J.W. Hopkins, C. J. Wohl, J.W. Connell, Optimized surface treatment of aerospace composites using a picosecond laser, Compos. B Eng. 175 (2019) 107155, https://doi.org/10.1016/j.compositesb.2019.107155.
[55] K. Sugioka, Progress in ultrafast laser processing and future prospects, Nanophotonics 6 (2) (2017) 393–413, https://doi.org/10.1515/NANOPH-2016-0004.
[56] A. Wolynski, T. Herrmann, P. Mucha, H. Haloui, J. L’huillier, Laser ablation of CFRP using picosecond laser pulses at different wavelengths from UV to IR, Phys. Procedia 12 (2011) 292–301, https://doi.org/10.1016/j.phpro.2011.03.136.
[57] V. Bhaskar, D. Kumar, K.K. Singh, Laser processing of glass fiber reinforced composite material: a review, Aust. J. Mech. Eng. 17 (2) (2019) 95–108, https://doi.org/10.1080/14484846.2017.1363989.
[58] J. Cheng, J. Liao, Z. Yang, F. Xie, Y. Chen, H. Du, D. Liu, Laser stripping of functional coatings on glass fiber reinforced plastic substrate, Appl. Opt. 61 (27) (2022) 7867, https://doi.org/10.1364/AO.468960.
[59] J. Gu, X. Su, Y. Jin, W. Li, Z. Zeng, D. Zhang, J. Xu, B. Guo, Towards low-temperature laser paint stripping by photochemical mechanism on CFRP substrates, J. Manuf. Process. 85 (2023) 272–280, https://doi.org/10.1016/j.jmapro.2022.11.041.
[60] B. Rauh, S. Kreling, M. Kolb, M. Geistbeck, S. Boujenfa, M. Suess, K. Dilger, UV-laser cleaning and surface characterization of an aerospace carbon fibre reinforced polymer, Int. J. Adhes. Adhes. 82 (2018) 50–59, https://doi.org/10.1016/J.IJADHADH.2017.12.016.
[61] P. Karlitschek, G. Hillrichs, K.-F. Klein, Photodegradation and nonlinear effects in optical fibers induced by pulsed uv-laser radiation, Opt. Commun. 116 (1–3) (1995) 219–230, https://doi.org/10.1016/0030-4018(95)00057-F.
[62] K. Takahashi, M. Tsukamoto, S. Masuno, Y. Sato, H. Yoshida, K. Tsubakimoto, H. Fujita, N. Miyanaga, M. Fujita, H. Ogata, Influence of laser scanning conditions on CFRP processing with a pulsed fiber laser, J. Mater. Process. Technol. 222 (2015) 110–121, https://doi.org/10.1016/j.jmatprotec.2015.02.043.
[63] D. Zhang, J. Xu, Z. Li, K. Li, C. Wang, D. Shan, B. Guo, Removal mechanism of blue paint on aluminum alloy substrate during surface cleaning using nanosecond pulsed laser, Opt. Laser Technol. 149 (2022) 107882, https://doi.org/10.1016/J.OPTLASTEC.2022.107882.
[64] D.C. Kirsch, S. Chen, R. Sidharthan, Y. Chen, S. Yoo, M. Chernysheva, Short-wave IR ultrafast fiber laser systems: Current challenges and prospective applications, J. Appl. Phys. 128 (18) (2020), https://doi.org/10.1063/5.0023936.
[65] J. Schille, U. Loeschner, Ultrashort pulse lasers in high-rate laser micro processing – Quo vadis? Advanced Optical Technologies 10 (4–5) (2021) 233–237, https://doi.org/10.1515/aot-2021-0049.
[66] J.-E. Kim, J.-M. Lee, J.-H. Hyun, J.-H. Jeong, J.-D. Kim, A Study on the Laser Removal of Epoxy Coatings on SS400 Surface by Beam Scanning Patterns, Coatings 11 (12) (2021) 1510, https://doi.org/10.3390/coatings11121510.
[67] J.-E. Kim, M.-K. Song, M.-S. Han, J.-D. Kim, A study on the application of laser cleaning process in shipbuilding industries using 100 W fiber laser, J. Mech. Sci. Technol. 35 (4) (2021) 1421–1427, https://doi.org/10.1007/s12206-021-0113-3.
[68] L. Liu, X. Liu, L. Kong, M. Wang, P. Hu, D. Wang, Effect of laser surface treatment on surface and bonding properties of carbon fiber reinforced composites, Int. J. Mater. Form. 13 (6) (2020) 885–895, https://doi.org/10.1007/s12289-019-01509-z.
[69] Y. Liu, W. Liu, D. Zhang, Z. Tian, X. Sun, Z. Wei, Experimental investigations into cleaning mechanism of ship shell plant surface involved in dry laser cleaning by controlling laser power, Appl. Phys. A 126 (11) (2020) 866, https://doi.org/10.1007/s00339-020-04050-y.
[70] Md. Shamsujjoha, S.R. Agnew, J.R. Brooks, T.J. Tyler, J.M. Fitz-Gerald, Effects of laser ablation coating removal (LACR) on a steel substrate: Part 2: Residual stress and fatigue, Surf. Coat. Technol. 281 (2015) 206–214, https://doi.org/10.1016/j.surfcoat.2015.02.034.
[71] Z. Tian, Z. Lei, X. Chen, Y. Chen, Evaluation of laser cleaning for defouling of marine biofilm contamination on aluminum alloys, Appl. Surf. Sci. 499 (2020) 144060, https://doi.org/10.1016/J.APSUSC.2019.144060.
[72] Z. Tian, J. Feng, X. Chen, Z. Lei, Y. Chen, Hybrid laser cleaning characteristic of marine barnacles fouling attached on Al alloys, J. Laser Appl. 33 (4) (2021) 042036, https://doi.org/10.2351/7.0000424.

[73] D. Ciofini, M. Martínez-Weinbaum, M. Castillejo, M. Oujja, C. Chillé, S. Siano, I. Osticioli, Quantitative spectroscopic characterization of laser-induced effects on oil paint films using 213, 266, or 2940 nm, J. Cult. Herit. 66 (2024) 155–165, https://doi.org/10.1016/j.culher.2023.11.015.
[74] S. Samolik, M. Walczak, M. Plotek, A. Sarzynski, I. Pluska, J. Marczak, Investigation into the removal of graffiti on mineral supports: Comparison of nanosecond Nd:YAG laser cleaning with traditional mechanical and chemical methods, Stud. Conserv. 60 (2015) S58–S64, https://doi.org/10.1179/0039363015Z.000000000208.
[75] S. Kalpakjian, S. Schmid, V. Sekar, Manufacturing Engineering and Technology, (7th edition)., Pearson Publications, 2013.
[76] M.P. Groover, Fundamentals of Modern Manufacturing: Materials, Processes, and Systems (Fourth Edition), John Wiley & Sons Inc, 2010.
[77] UNE-EN ISO 25178-2:2013 Especificación geométrica de productos... (n.d.). Retrieved December 26, 2021, from https://www.une.org/encuentra-tu-norma/busca-tu-norma/norma?c=N0051160.
[78] UNE-EN 828:2013 Adhesivos. Mojabilidad. Determinación por medi... (n.d.). Retrieved December 26, 2021, from https://www.une.org/encuentra-tu-norma/busca-tu-norma/norma?c=N0051185.
[79] Nandiyanto, A. B. D., Oktiani, R., & Ragadhita, R. (2019). How to Read and Interpret FTIR Spectroscope of Organic Material. Indonesian Journal of Science and Technology, 4(1), 97. 10.17509/ijost.v4i1.15806.
[80] M. Al-Amin, S. Chandra Dey, T.U. Rashid, M. Ashaduzzaman, S.M. Shamsuddin, Solar Assisted Photocatalytic Degradation of Reactive Azo Dyes in Presence of Anatase Titanium Dioxide, International Journal of Latest Research in Engineering and Technology 2 (2016) 14–21.
[81] M. Simon, A. Vianello, Y. Shashoua, J. Vollertsen, Accelerated weathering affects the chemical and physical properties of marine antifouling paint microplastics and their identification by ATR-FTIR spectroscopy, Chemosphere 274 (January) (2021) 129749, https://doi.org/10.1016/j.chemosphere.2021.129749.
[82] M. Lagerström, E. Ytreberg, A.-K.-E. Wiklund, L. Granhag, Antifouling paints leach copper in excess – study of metal release rates and efficacy along a salinity gradient, Water Res. 186 (2020) 116383, https://doi.org/10.1016/j.watres.2020.116383.
[83] C.A. Paz-Villarraga, Í.B. Castro, G. Fillmann, Biocides in antifouling paint formulations currently registered for use, Environ. Sci. Pollut. Res. 29 (20) (2022) 30090–30101, https://doi.org/10.1007/s11356-021-17662-5.
[84] F.B. Reig, J.V.G. Adelantado, M.C.M. Moya Moreno, FTIR quantitative analysis of calcium carbonate (calcite) and silica (quartz) mixtures using the constant ratio method, Application to Geological Samples. Talanta 58 (4) (2002) 811–821, https://doi.org/10.1016/S0039-9140(02)00372-7.
[85] P.K. Raul, S. Senapati, A.K. Sahoo, I.M. Umlong, R.R. Devi, A.J. Thakur, V. Veer, CuO nanorods: A potential and efficient adsorbent in water purification, RSC Adv. 4 (76) (2014) 40580–40587, https://doi.org/10.1039/c4ra04619f.
[86] M. Shafiey Dehaj, M. Zamani Mohiabadi, Experimental study of water-based CuO nanofluid flow in heat pipe solar collector, J. Therm. Anal. Calorim. 137 (6) (2019) 2061–2072, https://doi.org/10.1007/s10973-019-08046-6.
[87] M.R. Johan, M.S.M. Suan, N.L. Hawari, H.A. Ching, Annealing effects on the properties of copper oxide thin films prepared by chemical deposition, Int. J. Electrochem. Sci. 6 (12) (2011) 6094–6104, https://doi.org/10.1016/s1452-3981(23)19665-9.
[88] A. Artesani, F. Gherardi, A. Nevin, G. Valentini, D. Comelli, A photoluminescence study of the changes induced in the zinc white pigment by formation of zinc complexes, Materials 10(4)340 (2017), https://doi.org/10.3390/ma10040340.
[89] G.A. Bowmaker, J.V. Hanna, IR Spectroscopy of Two Polymorphs of Copper(I) Thiocyanate and of Complexes of Copper(I) Thiocyanate with Thiourea and Ethylenethiourea, Zeitschrift Fur Naturforschung - Section B Journal of Chemical Sciences 64 (11–12) (2009) 1478–1486, https://doi.org/10.1515/znb-2009-11-1231.
[90] A. Moreno, A.J. López, J. Lamas, A. Ramil, Femtosecond pulsed laser ablation for paint removal at oblique illumination: Effect of the incidence angle, Optik 264 (June) (2022) 169428, https://doi.org/10.1016/j.ijleo.2022.169428.
[91] K. Ziętkowska, R. Kozera, B. Przybyszewski, A. Boczkowska, B. Sztorch, D. Pakuła, B. Marciniec, R.E. Przekop, Hydro- and Icephobic Properties and Durability of Epoxy Gelcoat Modified with Double-Functionalized Polysiloxanes, Materials 16 (2) (2023) 875, https://doi.org/10.3390/ma16020875.
[92] R. Ellerbrock, M. Stein, J. Schaller, Comparing amorphous silica, short-range-ordered silicates and silicic acid species by FTIR, Sci. Rep. 12 (1) (2022) 1–8, https://doi.org/10.1038/s41598-022-15882-4.
[93] D.B. Mawhinney, J.A. Glass, J.T. Yates, FTIR study of the oxidation of porous silicon, J. Phys. Chem. B 101 (7) (1997) 1202–1206, https://doi.org/10.1021/jp963322r.
[94] A. Riveiro, A.L.B. Maçon, J. del Val, R. Comesaña, J. Pou, Laser surface texturing of polymers for biomedical applications, Front. Phys. 5 (FEB) (2018), https://doi.org/10.3389/fphy.2018.00016.
[95] D. Sola, R. Cases, High-repetition-rate femtosecond laser processing of acrylic intra-ocular lenses, Polymers 12 (1) (2020) 1–9, https://doi.org/10.3390/polym12010242.
[96] J. Brand, A. Wain, A.V. Rode, S. Madden, P.L. King, L. Rapp, Femtosecond pulse laser cleaning of spray paint from heritage stone surfaces, Opt. Express 30 (17) (2022) 31122, https://doi.org/10.1364/oe.468750.
[97] E. Almeida, T. Diamantino, O. de Sousa, Marine paints: The particular case of antifouling paints, Prog. Org. Coat. 59 (1) (2007) 2–20, https://doi.org/10.1016/J.PORGCOAT.2007.01.017.
[98] D. Quéré, Rough ideas on wetting, Physica A 313 (1–2) (2002) 32–46, https://doi.org/10.1016/S0378-4371(02)01033-6.
[99] Al Balushi, K.M., Sefiane, K., & Orejon, D, Binary mixture droplet wetting on micro-structure decorated surfaces, J. Colloid Interface Sci. 612 (2022) 792–805, https://doi.org/10.1016/j.jcis.2021.12.171.
[100] A. Marmur, Wetting on Hydrophobic Rough Surfaces: To Be Heterogeneous or Not To Be? Langmuir 19 (20) (2003) 8343–8348, https://doi.org/10.1021/LA0344682.
[101] S. Banerjee, Simple derivation of Young, Wenzel and Cassie-Baxter Equations and Its Interpretations. (2008). http://arxiv.org/abs/0808.1460.
[102] M. Nosonovsky, B. Bhushan, Superhydrophobic surfaces and emerging applications: Non-adhesion, energy, green engineering, Curr. Opin. Colloid Interface Sci. 14 (4) (2009) 270–280, https://doi.org/10.1016/j.cocis.2009.05.004.
[103] A.J. López, J.S. Pozo-Antonio, A. Moreno, T. Rivas, D. Pereira, A. Ramil, Femtosecond laser texturing as a tool to increase the hydrophobicity of ornamental stone: The influence of lithology and texture, Journal of Building Engineering 51 (2022) 104176, https://doi.org/10.1016/j.jobe.2022.104176.
[104] A.J. López, A. Ramil, J.S. Pozo-Antonio, T. Rivas, D. Pereira, Ultrafast laser surface texturing: A sustainable tool to modify wettability properties of marble, Sustainability 11 (15) (2019) 4079, https://doi.org/10.3390/su11154079.